



Published in final edited form as:

Nat Immunol. 2010 March ; 11(3): 232–239. doi:10.1038/ni.1842.

TRPV2 plays a pivotal role in macrophage particle binding and phagocytosis

Tiffany M. Link^{1,2,5}, Una Park^{1,2,5}, Becky M. Vonakis³, Daniel M. Raben¹, Mark J. Soloski⁴, and Michael J. Caterina^{1,2,5,6}

¹Department of Biological Chemistry, Johns Hopkins School of Medicine, Baltimore, MD 21205

²Department of Neuroscience, Johns Hopkins School of Medicine, Baltimore, MD 21205

³Department of Medicine Division of Allergy and Clinical Immunology, Johns Hopkins School of Medicine, Baltimore, MD 21205

⁴Department of Medicine Division of Rheumatology, Johns Hopkins School of Medicine, Baltimore, MD 21205

⁵Center for Sensory Biology, Johns Hopkins School of Medicine, Baltimore, MD 21205

Abstract

Macrophage phagocytosis is critical for defense against pathogens. Whereas many steps of phagocytosis involve ionic flux, the underlying ion channels remain ill-defined. Here, we show that zymosan-, IgG-, and complement-mediated particle binding and phagocytosis are impaired in macrophages lacking the cation channel, Transient Receptor Potential Vanilloid 2 (TRPV2). TRPV2 is recruited to the nascent phagosome and depolarizes the plasma membrane. Depolarization increases phosphatidylinositol-4,5-bisphosphate (PIP₂) synthesis, triggering the partial actin depolymerization necessary for occupancy-evoked phagocytic receptor clustering. TRPV2 knockout macrophages are also defective in chemoattractant-evoked motility. Consequently, TRPV2 knockout mice exhibit accelerated mortality and increased organ bacterial load when challenged with *Listeria monocytogenes*. These data reveal the participation of TRPV2 in early phagocytosis and its fundamental importance in innate immunity.

The phagocytic engulfment of invading microorganisms and foreign material by macrophages and other leukocytes is a key component of innate immunity. This process

Users may view, print, copy, download and text and data- mine the content in such documents, for the purposes of academic research, subject always to the full Conditions of use: http://www.nature.com/authors/editorial_policies/license.html#terms

⁶ Corresponding author 725 N. Wolfe Street Baltimore, MD 21205 caterina@jhmi.edu Phone: 410-502-5457 Fax: 410-955-5759.
Author Contributions

TML performed most of the experiments. UP generated TRPV2 KO mice, performed some immunolocalization experiments and contributed to study design. BAV contributed to study design regarding in vitro macrophage characterization and pathway dissection. MJS contributed to study design regarding *Listeria* experiments and interpretation of flow cytometry data. DMR contributed to study design regarding phospholipid metabolism. MJC performed some immunolocalization. TML and MJC designed the study, analyzed data and wrote the manuscript. All authors discussed the results and commented on the manuscript.

Supplementary Information is linked to the online version at.....

Supplementary Materials and Methods are linked to the online version at....

Competing Financial Interests

MJC is an inventor on a patent for the use of the TRPV2 DNA sequence

begins with receptor binding to intrinsic components of the particle or to IgG or complement opsonins on the particle surface. Occupied phagocytic receptors then trigger a series of complex intracellular signaling events to orchestrate efficient particle internalization^{1, 2}. While the details of this process vary, depending on the substrate being internalized and the receptors involved, one common feature is the clustering of occupied receptors to enhance substrate binding avidity in the phagosome^{3, 4}. Many steps in phagosome formation and maturation involve ionic flux across the plasma or phagosomal membrane^{2, 5-7}. Although some of the ion channels involved in these events have been identified, much remains to be learned about which particular channels are performing which specific functions in this process.

Transient Receptor Potential Vanilloid 2 (TRPV2) (A000811) is a nonselective cation channel expressed in macrophages, sensory neurons, and many other cell types that can be activated by diverse stimuli including noxious heat, cannabinoids, and phosphatidylinositol-3-OH kinase (PI(3)K) signaling⁸⁻¹². Previous studies have reported impairments in evoked cell migration, as well as alterations in Ca²⁺ influx evoked by formyl peptides or lysophospholipids, following siRNA knockdown of TRPV2 in TtT/M87 macrophage-derived cells or PC3 prostate cancer-derived cells^{13, 14}. Still, very little is known about the biological functions of this channel in macrophages or elsewhere. Here, we demonstrate that TRPV2 is a key participant in the earliest steps of macrophage phagocytosis. Macrophages in which this channel has been genetically eliminated or pharmacologically blocked are deficient in binding and internalization of a wide range of phagocytic substrates. Consistent with these findings, TRPV2 null mice exhibit accelerated mortality upon challenge with pathogenic *Listeria monocytogenes*.

RESULTS

TRPV2 expression and calcium influx responses in macrophages

To examine TRPV2 function in macrophages, we compared these cells between wild-type and TRPV2 knockout (KO) mice in which the TRPV2 gene has been globally disrupted (Park U., Vastani N., Guan Y., Raja S.N., Koltzenburg M., and Caterina M.J., *Submitted.*). Comparable numbers of resident macrophages, as well as monocytes, neutrophils and lymphocytes, were observed in peritoneal lavages from wild-type and TRPV2KO mice (Supplementary Fig. 1a,b). TRPV2 immunoreactivity was observed in cultured, adherent wild-type peritoneal macrophages, in apparently intracellular loci, as well as on the leading edge of polarized cells, but was absent from TRPV2KO macrophages (Fig. 1a). TRPV2 expression in wild-type but not TRPV2KO macrophages was confirmed by immunoblot (Fig. 1b). No differences in morphology or in F4/80 or F-actin staining were noted between genotypes (Fig. 1a, Supplementary Fig. 1c). TRPV2 immunoreactivity was also seen in liver Kupffer cells, skin epidermal Langerhans cells, and lung alveolar macrophages, in wild-type but not in TRPV2KO mice (Fig. 1c,d,e). These findings support the notion that TRPV2 is found in many resident macrophage populations.

Consistent with the expression of TRPV2 in these cells, fura-2 ratiometric imaging revealed a biphasic increase in intracellular Ca²⁺ in wild-type peritoneal macrophages stimulated with the TRPV2 agonist, ⁹-tetrahydrocannabinol (THC, 50 μM)¹¹ (Fig. 2a). Although basal

fura-2 ratios were comparable between wild-type and TRPV2KO macrophages, and cells of both genotypes often exhibited the first transient Ca^{2+} response, only wild-type cells displayed the larger, sustained response. Accordingly, maximal Ca^{2+} changes from baseline over the entire recording period were significantly smaller in TRPV2KO cells. Unlike THC, ATP (100 μM) (Fig. 2b) and formyl peptide (fMLP, 20 μM not shown) evoked comparable Ca^{2+} responses in wild-type and TRPV2KO macrophages. Ruthenium red (RR, 10 μM), an antagonist of TRPV2 and several other TRP channels¹⁵, reduced THC-evoked Ca^{2+} responses in wild-type macrophages to near the TRPV2KO level, but had no effect in TRPV2KO cells (Fig. 2c). THC-evoked Ca^{2+} increases were virtually ablated in the absence of extracellular Ca^{2+} , indicating that TRPV2 mediates a THC-evoked Ca^{2+} influx. AM251 (100 nM) and JTE 907 (100 nM), two selective antagonists of the G protein-coupled THC receptors, CB1 and CB2, respectively, reduced the residual THC-evoked Ca^{2+} response in TRPV2KO cells by 58%, but reduced the wild-type response by only 25%. These findings demonstrate that TRPV2 mediates THC-evoked Ca^{2+} influx and that THC action on TRPV2 is likely to be direct, rather than through CB1 or CB2.

Evoked motility and cytokine release in TRPV2 deficient macrophages

siRNA knockdown of TRPV2 in TtT/M87 cells or PC3 prostate cancer-derived cells reduces chemoattractant-evoked cell motility^{13, 14}. We observed a similar phenotype in primary TRPV2KO macrophages (Fig. 2d). In a filter migration assay, TRPV2KO macrophages exhibited reduced evoked migration towards 10% fetal calf serum (FCS), colony stimulating factor 1 (CSF1), or monocyte chemoattractant protein 1 (MCP1). A small, but significant deficit was also observed with 0.1% FCS on both sides of the filter. In contrast, there were no differences between wild-type and TRPV2KO macrophages in TNF release evoked by lipopolysaccharide, either with or without interferon γ (IFN γ) priming (Fig. 2e). Thus, TRPV2 contributes to cell motility in macrophages, but is not required for lipopolysaccharide-evoked TNF release.

Impaired Phagocytosis in TRPV2 deficient macrophages

We next addressed the potential involvement of TRPV2 in a more specialized macrophage function, phagocytosis. Within 5 min of exposure to IgG-coated latex beads (2 μm), adherent wild-type macrophages exhibited substantial phagocytosis, with most cells having engulfed > 6 beads (Fig. 3a,b). Bead internalization was confirmed by resistance to proteolytic removal (Supplementary Fig. 2). By comparison, TRPV2KO macrophages exhibited dramatically reduced phagocytosis. At 5 min, more than half of the TRPV2KO cells remained devoid of beads (Fig. 3a,b). This resulted in an 82.6% lower phagocytic index in TRPV2KO macrophages (Fig. 3d). Similar results were seen in bone marrow-derived macrophages (BMM) (Supplementary Fig. 3). We also measured macrophage binding of IgG-coated beads in the presence of cytochalasin D (10 μM), which blocks internalization by depolymerizing actin. After a 5 min incubation, ~90% of wild-type cells were associated with one or more beads (Fig. 3c) and these could be efficiently removed by proteolysis (Supplementary Fig. 2). In contrast, > 60% of TRPV2KO macrophages had no bound beads at this time point (Fig. 3c) and the overall distribution was again shifted towards lower numbers. This was reflected in a 76.5% lower binding index in TRPV2KO cells (Fig. 3e). RR (10 μM) inhibited both binding and phagocytosis of IgG-coated beads in

wild-type cells. Wild-type binding was also reduced by 2-trifluoromethylphenyl imidazole (TRIM), an antagonist of both TRPV2 and store-operated Ca^{2+} channels¹⁶ (Binding indices: wild-type, 0.43 ± 0.02 vs. wild-type+TRIM, 0.11 ± 0.01 , $n = 3$, $p < 10^{-4}$). TRPV2KO macrophages and RR-pretreated wild-type macrophages were also deficient in phagocytosis and binding of zymosan particles and complement-coated latex beads (Fig. 3d,e). These findings support an acute requirement for TRPV2 in the binding of diverse phagocytic substrates.

PI(3)K dependent TRPV2 recruitment to phagosomes

At baseline, under serum-free conditions, TRPV2 was diffusely expressed in a punctate pattern throughout the macrophage (Fig. 4a). Within 5 min of IgG-coated latex bead addition, TRPV2 became enriched around early phagosomes. TRPV2 also became enriched around phagosomes under binding conditions (i.e., 5 min in the presence of 10 μM cytochalasin D). Application of BSA-coated beads for 5 min did not result in bead binding or evoke changes in TRPV2 sub-cellular localization, excluding that the mechanical stimulation the bead may elicit could be the cause of TRPV2 recruitment (data not shown). In multiple cell types, TRPV2 is recruited to the plasma membrane in response to PI(3)K activation^{9, 13, 14}. Since this enzyme is activated during binding of IgG, complement, or zymosan to their respective phagocytic receptors¹⁷⁻¹⁹, and since it regulates early phagosome formation²⁰, we examined the potential involvement of PI(3)K in TRPV2 recruitment to phagosomes. The PI(3)K inhibitors, wortmannin (100 nM, Supplementary Fig. 4) and LY294002 (25 μM , Fig. 4a,b), each prevented TRPV2 recruitment to the nascent phagosome. Wortmannin (100 nM) also reduced the binding index of wild-type cells to IgG-coated beads to a level near that of TRPV2KO cells (Control wild-type, 0.43 ± 0.02 ; wild-type+wortmannin, 0.13 ± 0.01 , $p < 10^{-4}$ vs. control wild-type; TRPV2 KO, 0.11 ± 0.01 , $p < 10^{-4}$ vs. control wild-type). TRPV2 recruitment to phagosomes was also inhibited by the Src family kinase inhibitor PP2 (1 μM), Akt inhibitor X (10 μM), the general protein kinase C (PKC) inhibitor calphostin C (500 nM), and a PKC ζ -selective pseudosubstrate inhibitor (40 μM) (Fig. 4b). In contrast, neither the phospholipase C (PLC) inhibitor U73122 (10 μM), nor the Syk kinase inhibitor piceatannol (20 μM) affected TRPV2 recruitment, although all inhibitors decreased the number of beads phagocytosed at 5 min (data not shown). Thus, TRPV2 is recruited to nascent phagosomes during early phagocytosis by a pathway involving Src kinase, PI3 kinase, Akt, and PKC ζ signaling.

TRPV2 regulates Fc γ Receptor Clustering

Flow cytometry revealed that the broad binding and phagocytosis deficits in TRPV2KO macrophages were not attributable to differences in the functional surface expression of the major Fc γ or CR3 receptor subtypes^{21, 22}(Supplementary Fig. 5). An alternative way in which TRPV2 could reinforce binding of phagocytic substrates to macrophages is by regulating the substrate-evoked clustering, and thereby the avidity of phagocytic receptors. We therefore examined the relationship between TRPV2 and Fc γ R clustering during macrophage exposure to IgG. TRPV2 and Fc γ R exhibited non-overlapping punctate distributions in untreated macrophages (Fig. 4c). Binding of IgG immune complex (IC) for 5 min at 4°C (to prevent internalization without using cytochalasin D) resulted in the development of large clusters of Fc γ receptors across the surface of the cell that were co-

localized with TRPV2. In contrast, monomeric IgG failed to stimulate either Fc γ R clustering or TRPV2- Fc γ R co-localization. IC-stimulated Fc γ R clustering was significantly reduced in TRPV2KO macrophages. Staining performed after 5 min binding of IgG-coated beads (Fig. 4c) or IgG-coated zymosan particles (not shown) in wild-type macrophages revealed phagosomal colocalization of Fc γ R and TRPV2. Fc γ R were also enriched in the few beads that were bound to TRPV2KO macrophages. Thus, TRPV2 is required for efficient Fc γ R clustering and becomes co-localized with Fc γ R during multimeric, but not monomeric, IgG exposure.

Role of TRPV2-mediated depolarization in phagocytosis

Previous studies have reported changes in macrophage intracellular Ca²⁺ (ref. no.²³) and membrane potential^{6, 24-26} during phagocytosis. As a nonselective cation channel⁸, TRPV2 might regulate receptor clustering and substrate binding by either or both mechanisms. We therefore assayed changes in membrane potential during engagement of phagocytic receptors using the potentiometric fluorescent dye, FLIPR blue. Exposure of wild-type macrophages to ICs evoked a slow fluorescence increase, indicative of membrane depolarization, that was often punctuated by step rises, and reached a plateau within ~12 min (Fig. 5a). TRPV2KO macrophages had a baseline fluorescence similar to wild-type, but exhibited a much smaller depolarization upon IC challenge. Wortmannin or RR diminished the wild-type depolarization response to a level similar to that in TRPV2KO macrophages, consistent with an acute role for PI(3)K-recruited TRPV2 in this response. Similar patterns of robust depolarization in wild-type macrophages and reduced depolarization in TRPV2KO macrophages were observed with uncoated, IgG-coated, and complement-coated zymosan particles (Fig. 5b). Removal of extracellular Ca²⁺, coupled with the chelation of intracellular Ca²⁺, slightly increased binding of IgG-coated beads or zymosan particles to wild-type macrophages (Fig. 5c). Thus, Ca²⁺ does not appear necessary for these early binding events, consistent with previous findings²³. Replacement of extracellular Na⁺ with the larger and generally less permeable cation, n-methyl d-glucamine (NMDG), significantly reduced zymosan-evoked depolarization (Fig. 5d), binding to either zymosan particles or IgG-coated beads (Fig. 5e), as well as IC-evoked Fc γ R clustering in wild-type macrophages (compare Fig. 6a IC + NMDG with Fig. 4c IC alone), highlighting the importance of depolarization in these early steps of phagocytosis.

Artificial depolarization evoked with KCl augments binding of fibronectin-coated particles and apoptotic cells to macrophages²⁵. We therefore assessed the impact of this intervention on our cells. Buffer supplementation with 50 mM KCl (but not NaCl, not shown) evoked a comparable level of depolarization in wild-type and TRPV2KO macrophages (Fig. 5a). KCl also reverted the binding and phagocytosis defects in TRPV2KO or RR-treated wild-type macrophages to wild-type control levels across all substrates tested (Fig. 3a-e) and restored IC-evoked formation of large Fc γ R clusters in TRPV2KO macrophages (Fig. 5f). Remarkably, the combination of KCl and monomeric IgG was sufficient to trigger Fc γ R clustering in wild-type and TRPV2KO macrophages and to trigger TRPV2 recruitment to these clusters in wild-type macrophages (Fig. 6a). These findings corroborate the notion that the TRPV2 requirement for phagocytic receptor clustering, binding, and phagocytosis derives from its depolarization of the plasma membrane. They also suggest that membrane

depolarization can overcome the requirement for multimeric occupancy to achieve Fc γ R clustering.

Clustering through phospholipid-dependent actin depolymerization

IgG binding defects in phosphatidylinositol-4-phosphate 5-kinase (PIP5K) γ deficient macrophages, which synthesize insufficient PIP2 during phagocytosis, could be rescued by low (but not high) doses of the actin polymerization inhibitor latrunculin B, suggesting that Fc γ R clustering requires PIP2-mediated partial actin depolymerization²⁷. To determine whether abnormalities in the same pathway could account for the TRPV2KO phenotype, we used rhodamine-phalloidin to quantify F-actin before and after IC stimulation (Fig. 6b, Supplementary Fig. 6). For this experiment we used BMM due to their more uniform morphology relative to that of peritoneal macrophages. While basal F-actin levels were comparable between wild-type and TRPV2KO BMM, IC stimulation evoked a greater decline in F-actin content in wild-type than in TRPV2KO BMM. Addition of KCl to TRPV2KO cells restored the extent of actin depolymerization to that seen in wild-type. In fact, KCl alone was sufficient to evoke a degree of actin depolymerization in TRPV2KO cells similar to that seen in IC-treated wild-type cells. Since KCl also rescues the TRPV2KO defect in binding IgG, we asked whether partially depolymerizing actin by a different means would have the same effect. Indeed, at low doses (50 nM), latrunculin A or cytochalasin D fully rescued the TRPV2KO defect in binding IgG-coated beads. Conversely, higher doses which interfere more profoundly with the actin cytoskeleton (Fig. 6c), failed to rescue the TRPV2KO defect and actually decreased binding to wild-type peritoneal macrophages, assayed at 4°C. Whereas low dose cytochalasin D alone failed to evoke either Fc γ R clustering or colocalization of TRPV2 with Fc γ R, the combination of 50 nM cytochalasin D pretreatment and monomeric IgG triggered both events (Fig. 6a). Cytochalasin D (50 nM) also restored IC-evoked and monomeric IgG-evoked Fc γ R clustering in TRPV2KO peritoneal macrophages (data not shown). Substitution of extracellular Na⁺ with NMDG, to inhibit depolarization, prevented IC-evoked Fc γ R clustering, as expected, but did not prohibit either TRPV2 colocalization with Fc γ R or Fc γ R clustering evoked by a combination of IC and cytochalasin D. These findings strongly suggest that actin depolymerization is the relevant downstream outcome of TRPV2-mediated depolarization during phagocytosis.

To determine whether TRPV2-mediated depolarization alters actin dynamics through effects on PIP2 levels, we measured incorporation of ³²P into PIP2 during IC (Fig. 6d) or KCl (Fig. 6e) stimulation. BMMs were used in these experiments because of the greater yield of macrophages from each mouse. Untreated wild-type and TRPV2KO BMM exhibited similar basal levels of ³²P labeled PIP2 (Fig. 6d). IC stimulation evoked a 32-fold increase in [³²P] PIP2 in wild-type macrophages within 2 min. In contrast, the increase in [³²P] PIP2 was 5 fold lower in TRPV2KO macrophages. When KCl (50 mM) was added to TRPV2KO macrophages, in the absence of IC, ³²P PIP2 increased to a level statistically indistinguishable from that of IC-stimulated wild-type cells. This demonstrates that depolarization, whether it be through IC or KCl, directly affects phospholipid metabolism. Given that labeling of PIP2 increased after KCl stimulation, we reasoned that depolarization may be acting at or upstream of PIP2 biosynthetic enzymes. Type II phosphatidylinositol 4-

kinase PI(4)K is essential for PIP2 synthesis and regulation of actin on phagosomal membranes during latex bead phagocytosis²⁸. Consistent with our prediction, pretreatment of TRPV2KO macrophages with the type II PI(4)K inhibitor adenosine(300 μ M; Fig. 6e) inhibited the KCl-evoked increase in ³²P incorporation. We next examined KCl-triggered actin depolymerization in the presence or absence of U73122 (10 μ M, to block PIP2 hydrolysis by PLC), 100 nM wortmannin (to block PI3 kinase), adenosine (300 μ M, to block PI4 kinase), or 3m3FBS (10 μ M, to activate PLC and thus diminish PIP2 levels) (Fig. 6f). Neither U73122 nor wortmannin affected F-actin content in untreated or KCl stimulated cells. In contrast, adenosine and 3m3FBS both slightly increased basal F-actin levels, and abolished KCl-mediated actin depolymerization. These data indicate that depolarization mediated by Fc γ R-dependent activation of TRPV2 or by exogenous KCl alters clustering of occupied Fc γ R by stimulating PIP2 synthesis and consequent partial actin depolymerization.

TRPV2 null mice show enhanced susceptibility to pathogenic bacteria

To explore the pathological significance of our findings, we examined macrophage responses to a pathogenic bacterium, *Listeria monocytogenes* in the presence and absence of TRPV2. Acutely harvested peritoneal lavage cells obtained from wild-type and TRPV2KO mice were incubated with live, complement-opsonized *Listeria* and assayed for bacterial internalization after 10 or 100 min. Wild-type macrophages exhibited *Listeria* uptake that increased linearly with time (Fig. 7a). In contrast, *Listeria* uptake by TRPV2KO macrophages was significantly reduced such that at 100 min, 13-fold fewer bacteria were isolated from these cells, compared with wild-type ($P < 0.001$, Two-way ANOVA with Bonferroni post-test, $n = 5$). Finally, we asked whether the absence of TRPV2 would impair the host response to *Listeria* infection *in vivo*. Wild-type mice challenged intraperitoneally with a lethal bacterial dose (4.5×10^6 per mouse) exhibited a median survival of 7 days (Fig. 7b). By comparison, TRPV2KO mice died significantly sooner (median survival 3 days, $P < 0.0001$, Logrank test, $n = 8$). To determine whether this effect was due to impaired bacterial clearance in the TRPV2KO mice versus an exceptionally deleterious host response, we measured bacterial load in the liver and spleen two days after infection with a lower bacterial dose (5×10^5 per mouse). Under these conditions, TRPV2KO mice exhibited an ~60-fold greater bacterial load in both organs (Fig. 7c), consistent with suppressed bacterial clearance by macrophages and consequent accumulation in parenchymal cells. Thus, host defense against pathogenic *Listeria* is significantly compromised by the absence of TRPV2.

DISCUSSION

Our findings reveal that TRPV2 participates in the very earliest steps of macrophage phagocytosis. In the specific case of Fc γ R-mediated phagocytosis, TRPV2 channels recruited to the nascent phagosome in response to initial Fc γ R engagement by IgG mediate membrane depolarization, which in turn triggers PIP2 synthesis and the consequent actin depolymerization required for efficient higher-order clustering of occupied Fc γ R. In the absence of such clustering binding, and thus phagocytosis of IgG-coated particles are impaired.

The molecular mediator(s) of macrophage depolarization evoked by phagocytic substrates have remained unclear. Fc γ receptor-evoked depolarization in J774 cells was shown to result predominantly from Na⁺ influx through a pathway selective for small monovalent cations. Similar depolarization responses were observed in phospholipid vesicles reconstituted with purified Fc γ receptor, prompting the suggestion that the receptor itself formed the channel²⁶. Other studies have reported that in response to immune complexes or prolonged artificial depolarization macrophages exhibit a relatively nonselective cationic current^{6, 24}. Similar currents were seen in response to reactive oxygen species or ADP-ribose, leading to speculation that the depolarization-evoked current might be mediated by TRPM2. However, the significant NMDG permeability of the current was not characteristic of TRPM2²⁴ and, in related microglia, depolarization evoked currents pharmacologically resemble TRPV1²⁹. Also potentially involved in these responses is the potassium channel ether-a-go-go-related gene (ERG), whose inhibition potentiates macrophage depolarization²⁵. We do not yet understand the relationship between depolarization responses mediated by TRPV2 and those reported in these other studies. However, the fact that KCl treatment rescues the depolarization, binding and phagocytosis defects in TRPV2 deficient macrophages suggests that other ion channels can circumvent the requirement for TRPV2, if properly engaged.

Although artificial membrane depolarization facilitates phagocytic receptor binding²⁵, the underlying mechanism is not clear. We found that depolarization achieved via TRPV2 or KCl increases PIP2 synthesis, apparently by directly or indirectly activating PI(4)K. The polyamine spermine also activates PI(4)K³⁰, thus potentiation of this enzyme by membrane depolarization might be attributable to local surface charge effects at the inner plasma membrane leaflet²⁰. Depolarization-evoked PIP2 synthesis can be inhibited by adenosine, which is more potent for type II PI(4)K than type III subtypes, and has previously been shown to block latex bead-evoked phagosomal PIP2 synthesis in J774 macrophage cells²⁸. However, we cannot exclude the possible involvement of other PI(4)K isoforms in this process. PIP2 promotes controlled actin depolymerization during phagocytosis²⁷. Our data indicate that this effect on actin is the basis by which depolarization promotes Fc γ R clustering. Similar effects of TRPV2-mediated depolarization on the cytoskeleton might underlie the defects in chemoattractant-evoked motility observed in the absence of TRPV2^{13, 14}.

Normally, higher-order Fc γ R clustering depends not only on controlled actin dynamics²⁷, but also on oligomeric occupancy of neighboring Fc γ Rs²¹. Consistent with this notion, neither monomeric IgG, KCl, nor low-dose actin depolymerizing agents alone were sufficient to trigger Fc γ R clustering or TRPV2 co-localization with Fc γ R in our experiments. However, when monomeric IgG was combined with either of the other two stimuli, both clustering and co-localization proceeded normally. This suggests that initial Fc γ R oligomerization is not essential for subsequent clustering, provided that partial actin depolymerization is achieved in another way. Yet, TRPV2 recruitment, which is required for normal IgG-evoked actin depolymerization in the absence of an exogenous depolarizing stimulus, appears to require oligomeric Fc γ R occupancy. We also show that TRPV2 recruitment to the nascent phagosome requires Src family kinase signaling, as well as signaling through PI(3)K, Akt, and PKC ζ . Although the exact sequence must be established, Src family kinase activation is one of the earliest events in Fc γ R signaling, and

triggers PI(3)K activation²¹, while Akt is generally recruited by PI(3)K-synthesized PIP3. PKC ζ , which is also required for PIP3-dependent GLUT4 translocation in adipocytes³¹, likely acts downstream of Akt.

In our experiments, we measured clustering of the low-affinity Fc γ R (Fc γ RII/ Fc γ RIII). These are the isotypes thought to be primarily responsible for Fc γ R-mediated phagocytosis of IgG opsonized substrates (Indik, 1995). Another isotype, Fc γ RI, can bind monomeric IgG2a with high affinity, but is typically saturated under physiological conditions. Since our experiments use mixed isotype IgG, further work is necessary to discern any contributions of Fc γ RI to the clustering we observed.

We cannot exclude additional roles for TRPV2 in phagocytosis beyond substrate binding. A recent proteomics study detected TRPV2 in early endosomal fractions purified from bone marrow-derived macrophages and J774 cells³². Another group identified a Ca²⁺ current in artificially enlarged early endosomes in HEK293 embryonic kidney-derived cells that shared biophysical features with TRPV2, leading them to speculate that TRPV2 or a similar channel facilitates early endosome fusion and maturation³³. Studies to evaluate later functions for TRPV2 in phagocytosis are therefore warranted.

The other major finding of our study is that mice lacking TRPV2 are profoundly defective in defense against *Listeria* infection, exhibiting both impaired bacterial clearance and accelerated mortality. These results, which might be attributable to both the phagocytosis and motility defects observed in TRPV2KO macrophages, support a critical role for this channel in early innate immunity against *Listeria* and, perhaps, other intracellular pathogens. The increased organ bacterial load in *Listeria* infected TRPV2KO mice also suggests that one or more of the multiple pathways by which *Listeria* enters nonphagocytic parenchymal cells³⁴ are TRPV2 independent. Together, these findings make TRPV2 an attractive potential target for the treatment of microbial infection and other inflammatory and immune conditions that involve macrophages.

METHODS

Generation of TRPV2 knockout mice

Generation of TRPV2KO mice is described elsewhere (Park U., Vastani N., Guan Y., Raja S.N., Koltzenburg M., and Caterina M.J., *Submitted*.) DNA encoding TRPV2 transmembrane domains 5 and 6 and the intervening loop was deleted, ablating channel function and detectable protein. To overcome perinatal lethality observed in TRPV2KO mice on 129S6 or C57BL/6 backgrounds, we generated wild-type and TRPV2KO F1 hybrids by crossing C57Bl6 TRPV2^{+/-} mice with 129S6 TRPV2^{+/-} mice. The resulting TRPV2KO mice appear healthy except for an ~10 % reduction in body weight. All procedures were conducted in accordance with Johns Hopkins IACUC Policies.

Reagents

Cell culture reagents were from Invitrogen and other chemicals from Sigma, unless otherwise stated. Antibodies were from eBioscience, unless otherwise stated.

Macrophage harvest and culture

Mice (6-12 weeks old) were CO₂ euthanized. Peritoneal cells withdrawn in RPMI 1640/10% fetal calf serum (FCS) were plated on glass coverslips (1 hr, 37°C) and rinsed. Of adherent cells, >99% were F4/80⁺ macrophages. Bone marrow cells were cultured in macrophage differentiation medium (RPMI, 10% FCS, 10% L929-conditional medium, 1% glutamax, 1% penicillin/streptomycin) and assayed after 7–10 d.

Immunoblotting

Macrophages were lysed in RIPA buffer and lysates subjected to polyacrylamide gel electrophoresis and immunoblot as described³⁵ using anti-TRPV2⁸ (1:500), anti-β-actin (Sigma, 1:5000) and horseradish peroxidase-conjugated anti-rabbit or anti-mouse IgG (Amersham, 1:5000).

Immunostaining

Formalin-fixed macrophages and cryostat sections from mice perfused with 4% paraformaldehyde were immunostained as described³⁵ using 1:100-1:1000 rabbit anti-TRPV2⁸, 1:100 rat anti-F4/80 (ATCC HB198 supernatant), 1:100 rat anti-CD16/32 (FcγRII/III), 1:800 goat anti-rabbit Cy3 (Jackson), 1:200 goat anti-rabbit Alexa fluor-488 (Invitrogen), 1:400 goat anti-rat Cy2 (Jackson), or 1:800 goat anti-rat Cy3 (Jackson).

Flow cytometry

Peritoneal lavage cells in PBS/2% BSA/FcγR block (anti-CD16/32, 0.5 μg/ml) were incubated with: fluorescein isothiocyanate-labeled anti-F4/80 (5 μg/ml), phycoerythrin-labeled anti-Gr1 (2 μg/ml), anti-CD18 (2 μg/ml), anti-CD64 (2 μg/ml), anti-CD11b (2 μg/ml), or anti-CD16/32 (2 μg/ml), or allophycocyanin-labeled anti-CD11b (2 μg/ml), anti-B220 (2 μg/ml), or anti-CD3 (2 μg/ml). FcγR block was omitted during Fcγ receptor analysis. Cells were analysed on a FACS Calibur using CellQuest (BD Biosciences) and FlowJo (TreeStar) software.

Calcium imaging

Intracellular Ca²⁺ was monitored in calcium imaging buffer (CIB) as described³⁵. RR, AM 251 (Tocris), and JTE 907 (Tocris), were introduced 20 min prior to stimulation and present thereafter. For zero calcium CIB, CaCl₂ was replaced with 10 mM ethylene glycol tetraacetic acid (EGTA), and NaCl was reduced to 120 mM.

Cell migration assay

After 24 hr in culture, adherent macrophages were loaded with carboxyfluorescein succinimidyl ester (Molecular Probes, 3 μM), detached, and resuspended in RPMI/0.1% FCS in medium. Macrophages (4 × 10⁴) in 250 μl RPMI/0.1% FCS were loaded on filters (Fluoroblok, Becton Dickinson, 3 μm pore) precoated with fibronectin. Each filter was placed in a well of a 24 well plate containing 800 μl RPMI / 0.1% FCS alone or supplemented with 10% FCS, 100 ng/ml CSF-1 or 100ng/ml MCP-1. Cells having migrated through the filter after 20 min at 37°C were photographed by fluorescence microscopy in

five fields per treatment, with the researcher blinded to genotype and treatment, and counted using ImageJ software (NIH).

Cytokine release assay

Adherent peritoneal macrophages were stimulated with vehicle (DMSO 0.02%), LPS, or LPS plus IFN γ for 24 hr. Supernatants assayed for TNF by colorimetric ELISA (R&D Systems).

Phagocytosis and binding of opsonized beads or zymosan particles

Polystyrene beads (Bangs Laboratories, 2 μ m) or zymosan particles (3 μ m) were coated with mouse IgG (Equitech Bio, 5 mg/ml) or complement (normal mouse serum diluted 1:1 in PBS) for 1 h at 37°C, rinsed, and reconstituted in RPMI. Particles were centrifuged (100 \times g, 1 min) onto acutely harvested peritoneal macrophages at a 10:1 ratio to synchronize binding and internalization. After 5 min at 37°C, nonadherent beads were removed with cold PBS and cells were fixed in 3.7% formalin, and stained with rhodamine-phalloidin (1 U/ml, Invitrogen), anti-CD11b, anti-F4/80, or anti-TRPV2. Fifteen fields were photographed by bright field and epifluorescence microscopy. Quantification of beads ingested/bound is based on 200 macrophages per condition per genotype, performed in duplicate.

Phagocytosis or binding index was calculated as: Index = ($\sum n P_n$)/600 from $n = 0$ to $n = 6$, where n = number of particles bound to or phagocytosed by a cell and P_n = percentage of cells having bound or phagocytosed n particles. The investigator was blinded to genotype and treatment during photography and quantification. Any inhibitors were added for 10-40 min at 37°C prior to particle addition. Ca²⁺-free experiments were performed in Ca²⁺-free CIB containing 10 mM EGTA, on cells loaded with BAPTA-AM (Molecular Probes, 100 μ M) for 40 min prior to particle addition. Where indicated, NaCl was replaced with N-methyl-D-glucamine (NMDG, 130 mM). Where indicated, an additional 50 mM KCl was added to CIB or medium.

Phagosomal translocation of TRPV2

IgG-coated beads or ICs were added at a 4-5:1 ratio to plated macrophages that were untreated at 37°C (phagocytosis), pretreated with cytochalasin D at 37°C (binding), or untreated at 4°C (binding). Inhibitors were added 20 min before bead stimulation. After washing in cold PBS, cells were fixed and stained with anti-CD16/32 and anti-TRPV2, and imaged by confocal microscopy.

IC induced Fc γ R clustering

Immune complexes (ICs) were prepared as described³⁶. ICs (100 μ g/ml final) or monomeric IgG (100 μ g/ml final) were incubated 5 min at 4°C with prechilled plated macrophages in CIB. Where appropriate, 50 mM KCl was added to cells before stimulation with IC or monomeric IgG. Cytochalasin D exposure or Na⁺ substitution with NMDG, was initiated 20 min before stimulation and maintained throughout the experiment. Fc γ R-IC complexes were visualized by staining fixed, non-permeabilized cells with anti-CD16/32. Approximately 100 cells from each of duplicate coverslips were photographed per condition per genotype, and

the fractional area of plasma membrane occupied by small (< 50 pixels) versus large (> 50 pixels) clusters was quantified using ImageJ software.

Phagocytosis-associated membrane depolarization

Macrophages on coverslips were loaded (30 min, 25°C) with flash luminescence plate reader (FLIPR)-Blue dye (Molecular Devices, 1:12 in CIB), transferred to 300 µl CIB, equilibrated at 35°C, and imaged by fluorescence microscopy during a 12 min stimulation with phagocytic substrates that included IC (100 µg/ml), zymosan particles, complement-opsonized zymosan, or IgG-opsonized zymosan (10⁶ particles in 15 µl CIB delivered to the heated bath). For experiments involving wortmannin, RR, or Na⁺ substitution by NMDG, cells were pretreated for 20 min and maintained in the presence of those agents during stimulation.

F- actin quantitation

BMMs attached to glass coverslips were stimulated with ICs, fixed, permeabilized, and stained with rhodamine-phalloidin²⁷. Epifluorescence ($n = 3$ mice/genotype/condition) was measured in ~100 cells per condition per genotype from 40 random fields in duplicate coverslips using ImageJ software. Investigator was blinded to genotype and treatment during photography and quantification.

³²P-labeling of phospholipids

BMM were labeled for 2-4 hrs with [³²P] disodium phosphate (10 µCi/ml, Perkin Elmer) in phosphate-free DMEM, stimulated for 2-10 min with KCl (50 mM final) or IC (100 µg/ml) at 37°C and rinsed. Acidified methanol (Methanol/HCl, 49.5:0.5, 1 ml) was added and the cells scraped. Acidified methanol/dH₂O/chloroform (1:0.8:1) was added, the organic phase was removed and the aqueous phase extracted with another 2 ml of chloroform. Organic phase samples were dried under N₂ and re-dissolved in chloroform/methanol (95:5). Lipids were separated by TLC on aluminum-backed silica gel G60 plates using a two solvent system³⁷. Plates were dried and radiolabeled lipids visualized by autoradiography. The PIP₂ band, localized by a parallel standard (Avanti), was excised and counted in CytoScint ES liquid scintillant (ICN Biomedicals). Counts were standardized to total lipid phosphate, measured as described³⁸.

Listeria monocytogenes phagocytosis *in vitro* and infection *in vivo*

Listeria Monocytogenes (LM, strain 43251), were grown to mid-logarithmic phase, pelleted, washed, and resuspended in PBS. Acutely harvested peritoneal lavage cells (100 µl at 2 × 10⁶ cells/ml) were added to 2 × 10⁵ LM in 100 µl PBS, and incubated for 15 or 100 min at 37°C. Cells were repeatedly rinsed with PBS to remove extracellular bacteria, and lysed with water to liberate intracellular bacteria. Serial dilutions were plated on brain heart infusion (BHI) agar plates. Bacterial colonies were counted 24 hr later. Mid-logarithmic phase LM were adjusted to the indicated concentration in PBS and 200 µl injected intraperitoneally per mouse. Animals were monitored daily for 10 days. For determination of bacterial burden of the liver and spleen, mice were sacrificed 48 hr post inoculation, organs were homogenized

in PBS, and serial dilutions of the homogenate plated on BHI agar plates, with colony counting 24 hr later.

Data analysis

Unless otherwise indicated, statistical comparisons were performed using Student's unpaired *t*-test and *p*-values reflect comparison with control wild-type sample. Where indicated, two-way ANOVA and Kaplan Meier survival analyses were conducted using Prism software (GraphPad).

Supplementary Material

Refer to Web version on PubMed Central for supplementary material.

Acknowledgements

The authors thank J. Brederson, M.-K. Chung, S. Huang, M. Meffert, C. Munns, and V. Vega for suggestions, J. Wang and S. Li for technical assistance, S. Hudson for help with flow cytometry, P. Devreotes for suggestions and Latrunculin A, and W. Bishai and S. Huang for critically reading the manuscript. Supported by grants from the NIH (R01NS051551 to MJC, RO1AI42287-05 to MJS, AI059298 and AI071117 to BMV, GM059251 to DMR, and a Medical Scientist Training Program Award to TML).

REFERENCES

1. Aderem A, Underhill DM. Mechanisms of phagocytosis in macrophages. *Annu. Rev. Immunol.* 1999; 17:593–623. [PubMed: 10358769]
2. Flannagan RS, Cosio G, Grinstein S. Antimicrobial mechanisms of phagocytes and bacterial evasion strategies. *Nat. Rev. Microbiol.* 2009; 7:355–366. [PubMed: 19369951]
3. Hackam DJ, Rotstein OD, Schreiber A, Zhang W, Grinstein S. Rho is required for the initiation of calcium signaling and phagocytosis by Fcγ receptors in macrophages. *J. Exp. Med.* 1997; 186:955–966. [PubMed: 9294149]
4. Jongstra-Bilen J, Harrison R, Grinstein S. Fcγ receptors induce Mac-1 (CD11b/CD18) mobilization and accumulation in the phagocytic cup for optimal phagocytosis. *J. Biol. Chem.* 2003; 278:45720–45729. [PubMed: 12941957]
5. Carrithers MD, et al. Expression of the voltage-gated sodium channel NaV1.5 in the macrophage late endosome regulates endosomal acidification. *J. Immunol.* 2007; 178:7822–7832. [PubMed: 17548620]
6. Holevinsky KO, Nelson DJ. Simultaneous detection of free radical release and membrane current during phagocytosis. *J. Biol. Chem.* 1995; 270:8328–8336. [PubMed: 7713941]
7. Mellman I, Fuchs R, Helenius A. Acidification of the endocytic and exocytic pathways. *Annu. Rev. Biochem.* 1986; 55:663–700. [PubMed: 2874766]
8. Caterina MJ, Rosen TA, Tominaga M, Brake AJ, Julius D. A capsaicin receptor homologue with a high threshold for noxious heat. *Nature.* 1999; 398:436–441. [PubMed: 10201375]
9. Kanzaki M, et al. Translocation of a calcium-permeable cation channel induced by insulin-like growth factor-I. *Nat. Cell Biol.* 1999; 1:165–170. [PubMed: 10559903]
10. Kowase T, Nakazato Y, Yoko OH, Morikawa A, Kojima I. Immunohistochemical localization of growth factor-regulated channel (GRC) in human tissues. *Endocrine J.* 2002; 49:349–355. [PubMed: 12201220]
11. Nepper MP, et al. Activation properties of heterologously expressed mammalian TRPV2: evidence for species dependence. *J. Biol. Chem.* 2007; 282:15894–15902. [PubMed: 17395593]
12. Penna A, et al. PI3-kinase promotes TRPV2 activity independently of channel translocation to the plasma membrane. *Cell Calcium.* 2006; 39:495–507. [PubMed: 16533525]

13. Monet M, et al. Lysophospholipids stimulate prostate cancer cell migration via TRPV2 channel activation. *Biochim. Biophys. Acta.* 2009; 1793:528–539. [PubMed: 19321128]
14. Nagasawa M, Nakagawa Y, Tanaka S, Kojima I. Chemotactic peptide fMetLeuPhe induces translocation of the TRPV2 channel in macrophages. *J. Cell Physiol.* 2007; 210:692–702. [PubMed: 17154364]
15. Ramsey IS, Delling M, Clapham DE. An Introduction to TRP Channels. *Annu. Rev. Physiol.* 2006; 8:619–47. [PubMed: 16460286]
16. Juvin V, Penna A, Chemin J, Lin YL, Rassendren FA. Pharmacological characterization and molecular determinants of the activation of transient receptor potential V2 channel orthologs by 2-aminoethoxydiphenyl borate. *Mol. Pharmacol.* 2007; 72:1258–1268. [PubMed: 17673572]
17. Herre J, et al. Dectin-1 uses novel mechanisms for yeast phagocytosis in macrophages. *Blood.* 2004; 104:4038–4045. [PubMed: 15304394]
18. Khandani A, et al. Microtubules regulate PI-3K activity and recruitment to the phagocytic cup during Fcγ receptor-mediated phagocytosis in nonelicited macrophages. *J. Leukocyte Biol.* 2007; 82:417–428. [PubMed: 17502337]
19. Li B, et al. Yeast beta-glucan amplifies phagocyte killing of iC3b-opsonized tumor cells via complement receptor 3-Syk-phosphatidylinositol 3-kinase pathway. *J. Immunol.* 2006; 177:1661–1669. [PubMed: 16849475]
20. Yeung T, et al. Receptor activation alters inner surface potential during phagocytosis. *Science.* 2006; 313:347–351. [PubMed: 16857939]
21. Garcia-Garcia E, Rosales C. Signal transduction during Fc receptor-mediated phagocytosis. *J. Leukocyte Biol.* 2002; 72:1092–1108. [PubMed: 12488490]
22. Ueda T, Rieu P, Brayer J, Arnaout MA. Identification of the complement iC3b binding site in the beta 2 integrin CR3 (CD11b/CD18). *Proc. Natl. Acad. Sci. USA.* 1994; 91:10680–10684. [PubMed: 7524101]
23. Di Virgilio F, Meyer BC, Greenberg S, Silverstein SC. Fc receptor-mediated phagocytosis occurs in macrophages at exceedingly low cytosolic Ca²⁺ levels. *J. Cell Biol.* 1988; 106:657–666. [PubMed: 3346321]
24. Campo B, Surprenant A, North RA. Sustained depolarization and ADP-ribose activate a common ionic current in rat peritoneal macrophages. *J. Immunol.* 2003; 170:1167–1173. [PubMed: 12538672]
25. Vernon-Wilson EF, et al. CD31 delays phagocyte membrane repolarization to promote efficient binding of apoptotic cells. *J. Leukocyte Biol.* 2007; 82:1278–1288. [PubMed: 17684043]
26. Young JD, Unkeless JC, Kaback HR, Cohn ZA. Mouse macrophage Fc receptor for IgG gamma 2b/gamma 1 in artificial and plasma membrane vesicles functions as a ligand-dependent ionophore. *Proc. Natl. Acad. Sci. USA.* 1983; 80:1636–1640. [PubMed: 6300861]
27. Mao YS, et al. Essential and unique roles of PIP5K-gamma and -alpha in Fcγ receptor-mediated phagocytosis. *J. Cell Biol.* 2009; 184:281–296. [PubMed: 19153220]
28. Defacque H, et al. Phosphoinositides regulate membrane-dependent actin assembly by latex bead phagosomes. *Mol. Biol. Cell.* 2002; 13:1190–1202. [PubMed: 11950931]
29. Schilling T, Eder C. Importance of the non-selective cation channel TRPV1 for microglial reactive oxygen species generation. *J. Immunol.* 2009
30. Etkovitz N, Rubinstein S, Daniel L, Breitbart H. Role of PI3-kinase and PI4-kinase in actin polymerization during bovine sperm capacitation. *Biol. Reprod.* 2007; 77:263–273. [PubMed: 17494916]
31. Ishiki M, Klip A. Minireview: recent developments in the regulation of glucose transporter-4 traffic: new signals, locations, and partners. *Endocrinology.* 2005; 146:5071–5078. [PubMed: 16150904]
32. Wainszelbaum MJ, Proctor BM, Pontow SE, Stahl PD, Barbieri MA. IL4/PGE2 induction of an enlarged early endosomal compartment in mouse macrophages is Rab5-dependent. *Exp. Cell. Res.* 2006; 312:2238–2251. [PubMed: 16650848]
33. Saito M, Hanson PI, Schlesinger P. Luminal chloride-dependent activation of endosome calcium channels: patch clamp study of enlarged endosomes. *J. Biol. Chem.* 2007; 282:27327–27333. [PubMed: 17609211]

34. Cossart P, Toledo-Arana A. *Listeria monocytogenes*, a unique model in infection biology: an overview. *Microbes Infect.* 2008; 10:1041–1050. [PubMed: 18775788]
35. Guler AD, et al. Heat-evoked activation of the ion channel, TRPV4. *J. Neurosci.* 2002; 22:6408–6414. [PubMed: 12151520]
36. Sobota A, et al. Binding of IgG-opsonized particles to Fc gamma R is an active stage of phagocytosis that involves receptor clustering and phosphorylation. *J. Immunol.* 2005; 175:4450–4457. [PubMed: 16177087]
37. Medh JD, Weigel PH. Separation of phosphatidylinositols and other phospholipids by two-step one-dimensional thin-layer chromatography. *J. Lipid Res.* 1989; 30:761–764. [PubMed: 2760549]
38. Ames BN, Dubin DT. The role of polyamines in the neutralization of bacteriophage deoxyribonucleic acid. *J. Biol. Chem.* 1960; 235:769–775. [PubMed: 13793161]

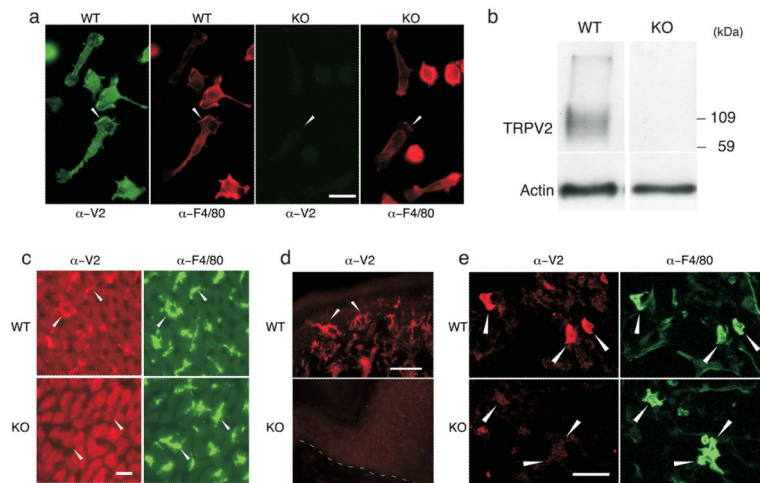


Figure 1.

TRPV2 expression in phagocyte populations. **(a)** TRPV2 immunofluorescence staining in resident peritoneal macrophages from wild-type but not TRPV2 knockout (KO) mice. Arrowheads highlight leading edge of polarized cells. Scale bar, 20 μm . **(b)** Immunoblot of WT and TRPV2KO peritoneal macrophages lysates stained with anti-TRPV2 (top) or anti- β -actin (bottom). A TRPV2-immunoreactive protein band is observed in lysates of wild-type peritoneal macrophages, but is absent from TRPV2KO lysates. Recombinant mouse TRPV2 has a molecular mass of ~ 92 kDa, consistent with this signal. The breadth of the band is likely attributable to TRPV2 glycosylation (4). **(c)** TRPV2 (red) and F4/80 (green) immunofluorescence staining in wild-type but not TRPV2KO liver Kupffer cells (arrowheads). Scale bar, 20 μm . **(d)** TRPV2 immunoreactivity (red) in wild-type but not TRPV2KO Langerhans cells (arrowheads) in tangential sections through the hind paw glabrous skin. Dashed line designates dermal-epidermal border. **(e)** TRPV2 immunoreactivity (red) in wild-type but not TRPV2KO lung alveolar macrophages (arrowheads) double labeled with F4/80 (green). Scale bar is 20 μm in panels **a**, **c**, and **e**, and 50 μm in panel **e**.

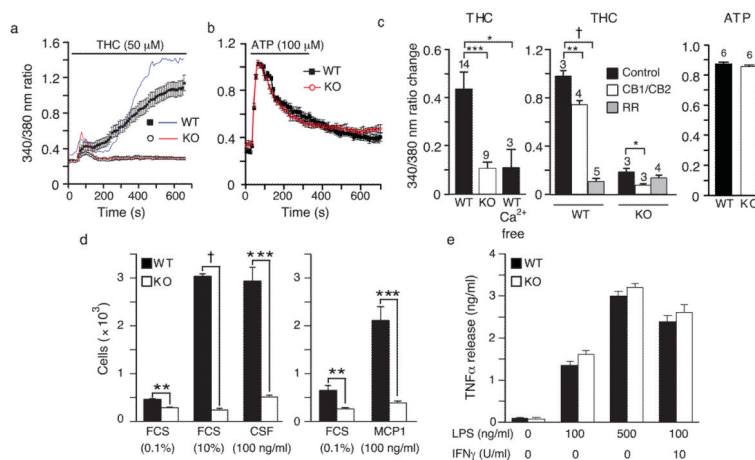
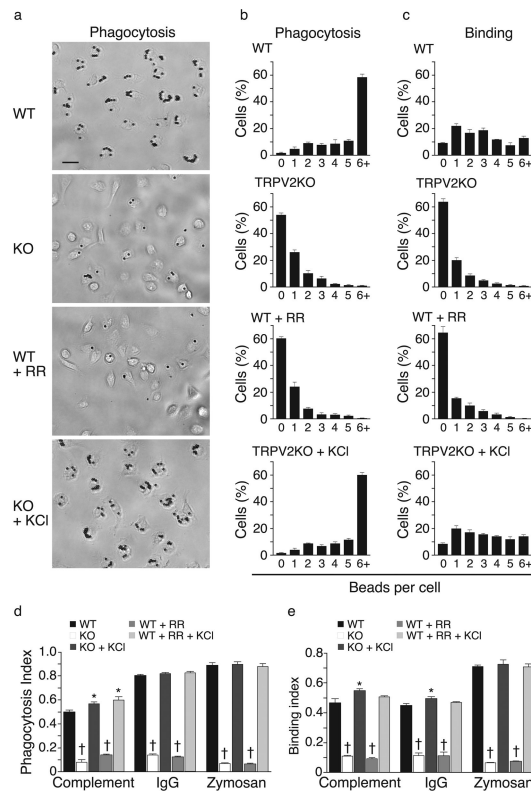


Figure 2. TRPV2 calcium influx responses and function in macrophage chemotaxis and cytokine release. **(a)** Single representative fura2 ratio traces (ratio of emission upon excitation at 340 nm/excitation at 380 nm) from THC (50 μ M)-stimulated wild-type (blue) and TRPV2KO (red) cells. Filled squares (wild-type) and open circles (TRPV2KO) indicate mean \pm SEM values from 50-100 cells on a single coverslip. **(b)** Filled black squares (wild-type) and open red circles (TRPV2KO) indicate mean \pm SEM fura ratios from 50-100 ATP (100 μ M)-stimulated cells on a single coverslip. Horizontal bars in panels a and b indicate stimulus period. **(c)** Mean \pm SEM changes in fura ratio (peak response minus baseline just prior to stimulation) evoked under the indicated conditions: Ca^{2+} free, Ca^{2+} absent from extracellular medium; CB1/CB2, AM251 and JTE 907, antagonists of CB1 and CB2 cannabinoid receptors, both at 100 nM; RR, ruthenium red, 10 μ M. Numerals indicate number of coverslips assayed. **(d)** Impaired basal and chemoattractant-evoked motility in peritoneal macrophages from TRPV2KO mice in a filter migration assay. Mean \pm SEM cells counted in 5 fields at the bottom surface of the filter. $n = 3$ pair of mice for FCS and $n = 4$ for MCP1 and CSF1. **(e)** TNF release is shown for wild-type (black bars) and TRPV2KO (white bars) macrophages after stimulation with vehicle (0.02% DMSO), 100 ng/ml LPS, 500 ng/ml LPS, or with IFN γ priming, followed by 100 ng/ml LPS. Mean \pm SEM, $n = 4$ mice per genotype assayed in triplicate. * $P < 0.05$, ** $P < 0.01$, *** $P < 0.001$, † $P < 10^{-4}$.

**Figure 3.**

Defective phagocytosis and particle binding across diverse substrates in TRPV2 knockout macrophages. **(a)** Representative photomicrographs of wild-type and TRPV2KO peritoneal macrophages following 5 min phagocytosis of IgG-coated latex beads (2 μ m). Top two photos show wild-type and TRPV2KO cells, respectively, exposed to beads under control conditions. In the third photo, wild-type cells were exposed to beads in the presence of ruthenium red (RR, 10 μ M). In the bottom photo, TRPV2KO cells were exposed to beads with KCl (50 mM) added to the medium. **(b)** Corresponding distributions of mean \pm SEM numbers of IgG-coated beads phagocytosed by individual cells in each genotype and treatment group. **(c)** Macrophage binding of IgG-coated latex beads, measured during a 5 min incubation in the presence of cytochalasin D (10 μ M) to prevent internalization, and expressed as mean \pm SEM number of bound particles per cell. **(d, e)** Phagocytic index **(d)** or Binding index **(e)** for IgG-coated beads, complement-coated beads, and zymosan particles under control conditions and in the presence of RR and/or KCl. In panels **(b-e)**, $n = 4$ mice per genotype, each assayed in duplicate. * $P < 0.05$, † $P < 10^{-4}$.

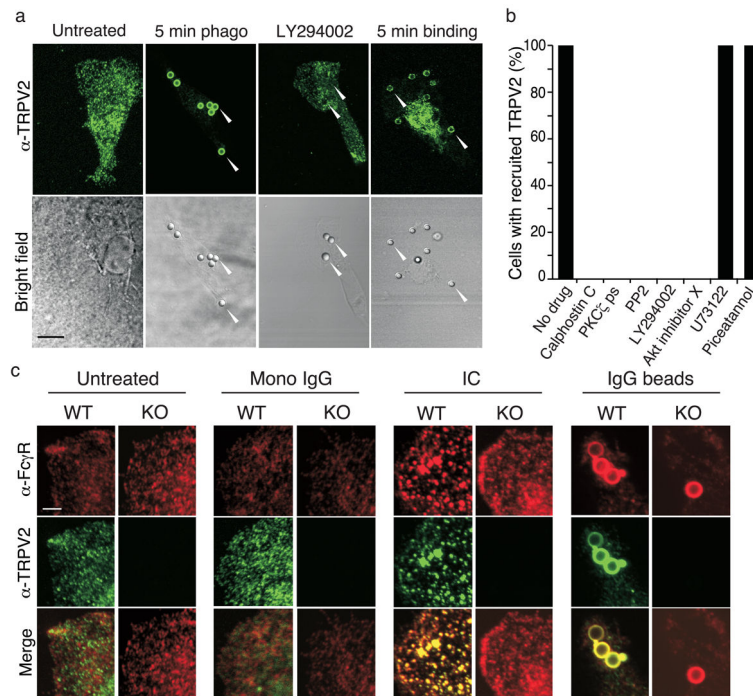
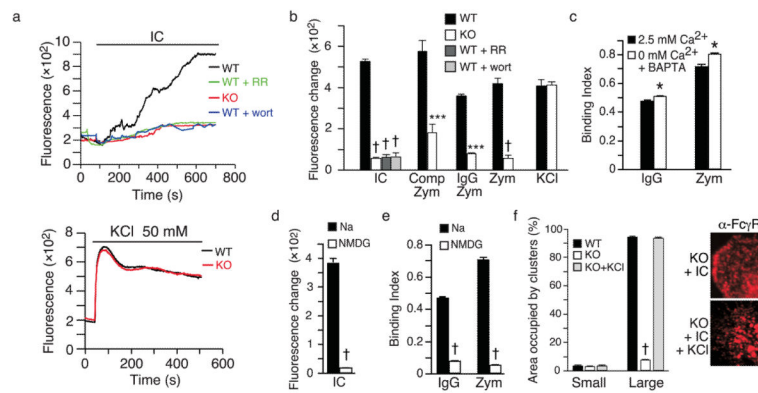


Figure 4.

TRPV2 translocation to developing phagosomes and Fc γ R clustering. **(a)** TRPV2 is recruited to the developing phagosome in a PI(3)K-dependent manner. Wild-type macrophages are shown at baseline, after 5 min phagocytosis of IgG-coated beads, after 5 min phagocytosis in the presence of LY294002 (25 μ M), or after 5 min binding of IgG-coated beads in the presence of cytochalasin D (10 μ M). Top, TRPV2 immunofluorescence. Bottom, brightfield images. Arrowheads highlight beads. Scale bar, 8 μ m. **(b)** Phagocytosis (5 min) of IgG-coated beads in wild-type macrophages, in the absence of drugs, or the presence of calphostin C (500 nM), PKC ζ pseudosubstrate (40 μ M), PP2 (1 μ M), LY294002 (25 μ M), Akt inhibitor X (10 μ M), U73122 (10 μ M), or piceatannol (20 μ M). The presence or absence of TRPV2 in phagosomes was quantified. Data expressed as percentage of cells with phagosomes containing TRPV2. At least 20 cells from each of 3 mice were assayed in duplicate. **(c)** TRPV2 colocalizes with the Fc γ R and is required for Fc γ R clustering. Wild-type and TRPV2KO macrophages at baseline, treated with monomeric IgG, IC, or IgG beads, for 2 min at 37°C. Scale bar, 4 μ m

**Figure 5.**

TRPV2-dependent depolarization regulates particle binding and Fc γ R clustering. Membrane depolarization evoked by IC, zymosan particles, or IgG- or complement-coated zymosan particles is impaired in TRPV2KO macrophages. **(a)** Membrane potential was measured using the voltage-sensitive dye, FLIPR blue, whose fluorescence increases at depolarized potentials. Top, responses of representative wild-type (black) and TRPV2KO (red) cells to IC and inhibition of wild-type response by RR (green, 10 μ M) or wortmannin (blue, 100 nM). Bottom, representative responses to KCl (50 mM). **(b)** Mean \pm SEM changes from baseline, $n = 5$ coverslips per genotype or treatment. **(c)** Effect of removal of extracellular Ca²⁺, coupled with chelation of intracellular Ca²⁺ with BAPTA, on binding of zymosan particles or IgG-coated latex beads. Mean \pm SEM, $n = 4$ wells per treatment. **(d, e)** Effects of extracellular Na⁺ replacement with NMDG on IC-evoked depolarization (**d**, $n = 6$ coverslips per treatment) and binding of IgG-coated beads (**e**, $n = 4$ wells per treatment). **(f)** Graph at left shows mean \pm SEM percent surface area of cell occupied by small (< 50 pixels) versus large (> 50 pixels) clusters in each IC-treated group. Right, representative images of Fc γ R stained TRPV2KO macrophages treated with IC or IC + KCl. $n = 3$ mice per genotype, assayed in duplicate. * $P < 0.05$, *** $P < 0.001$, † $P < 10^{-4}$.

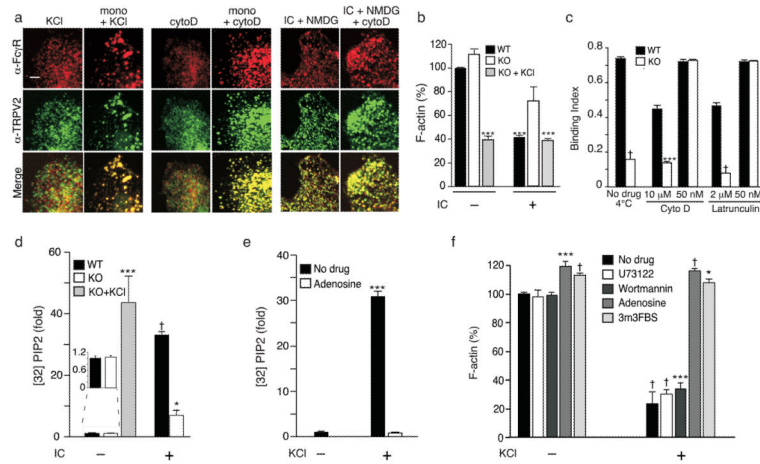


Figure 6.

Depolarization and actin depolymerization regulate Fc γ R clustering. **(a)** Fc γ R clustering regulation by depolarization and actin depolymerization. Representative images of wild-type macrophages treated as indicated: KCl, 50 mM KCl; mono, monomeric IgG; cytoD, pretreated with cytochalasin D (50 nM); NMDG, replacement of Na⁺ with NMDG. **(b)** IC-induced actin depolymerization. F-actin was quantitated using a fluorometric phalloidin-binding assay. Rhodamine-phalloidin intensity is expressed as a percentage of wild-type without IC, \pm SEM, $n = 3$ mice per condition per genotype, assayed in duplicate. Scale bar, 4 μ m. **(c)** Rescue of TRPV2KO defect in IgG-coated bead binding by partial inhibition of actin polymerization with low, but not high concentrations of latrunculin A or cytochalasin D. Binding without drugs at 4 $^{\circ}$ C serves as a control. Mean \pm SEM, $n = 3$ mice per condition per genotype, assayed in duplicate. **(d)** IC or KCl-induced changes in ³²P incorporation into PIP2, measured by TLC. **(e)** Effect of PI4 kinase inhibition on KCl-induced changes in ³²P incorporation into PIP2, measured by TLC. Adenosine (300 μ M) pretreatment of cells was used to inhibit type II PI(4)K before KCl stimulation. 3 mice per genotype per condition. ³²P incorporation is expressed as fold increase over untreated wild-type **(d)** and TRPV2KO **(e)**. **(f)** Effects of PIP2 metabolism on KCl-mediated actin depolymerization. F-actin was measured and quantified as in **b**, and expressed as a percentage of untreated TRPV2KO without KCl stimulation, \pm SEM. Drugs used: U73122 (10 μ M), wortmannin (100 nM), adenosine (300 μ M), and PLC activator 3m3FBS (10 μ M). $n = 3$ mice per condition, assayed in duplicate. * $P < 0.05$, ** $P < 0.01$, *** $P < 0.001$, † $P < 10^{-4}$.

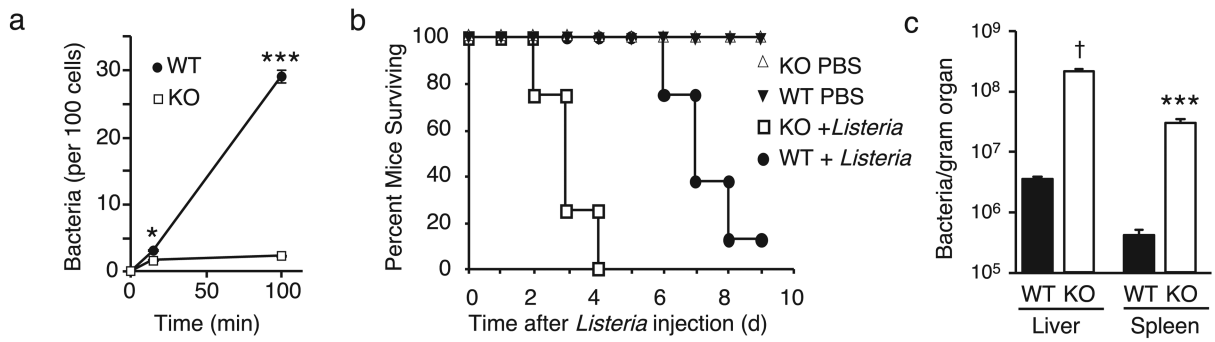


Figure 7.

Impaired bacterial phagocytosis by TRPV2 deficient macrophages *in vitro* and enhanced *in vivo* susceptibility of TRPV2KO mice to bacterial infection. (a) Quantification of *Listeria monocytogenes* internalized by acutely harvested wild-type and TRPV2KO peritoneal macrophages in suspension over the indicated time periods. Mean \pm SEM, $n = 5$ mice per genotype, assayed in duplicate. (b) Death curve in wild-type (closed circle) and TRPV2KO (open square) mice injected i.p. with 4.5×10^6 *Listeria* or vehicle (PBS). $n = 10$ per genotype. (c) Comparison of bacterial loads in spleen and liver of wild-type and TRPV2KO mice injected 48 hr earlier with 5×10^5 *Listeria*. * $P < 0.05$, *** $P < 0.001$, † $P < 10^{-4}$, $n = 5$ per genotype.